






Article

Negative Impact Mitigation on the Power Supply System of a Fans Group with Frequency-Variable Drive

Yerbol Yerbayev ¹, Ivan Artyukhov ^{2,*}, Artem Zemtsov ³, Denis Artyukhov ², Svetlana Molot ²,
Dinara Japarova ¹ and Viktor Zakharov ⁴

¹ Higher School of Electrical Engineering and Automation, Zhangir Khan West Kazakhstan Agrarian Technical University, Uralsk 090009, Kazakhstan

² Department of Power and Electrical Engineering, Yuri Gagarin State Technical University of Saratov, 410054 Saratov, Russia

³ Department of Power Supply for Industrial Enterprises, Samara State Technical University, Syzran Branch, 446001 Syzran, Russia

⁴ Department of Energy, Automation and Computer Technology, West Kazakhstan Innovative and Technological University, Uralsk 090009, Kazakhstan

* Correspondence: ivart54@mail.ru

Abstract: The technological installations' characteristics are possible to improve by equipping fans with a frequency-controlled electric drive. However, it can lead to an electromagnetic compatibility problem in the electrical supply system. This problem becomes worse if a large number of fans are included in the technological installation and the electric drives are powered from a substation connected to a limited power source. As an example, in this article we investigate the power supply system of a gas cooling unit with variable-frequency electric drives for fans. The electric drives' operating mode dependences characterizing the non-sinusoidal voltages and currents of the power source are obtained with the help of simulation modeling in the MATLAB environment with the Simulink expansion package. The typical substation circuit usage for the power supply of a group of fans with a frequency-controlled drive does not meet the requirements of IEEE Standard 519-2014. We can solve the problem of electromagnetic compatibility by changing the substation topology and organizing DC busbars and replacing frequency converters with inverters. We proposed forming DC busbars using 12-pulse rectifiers powered by transformers with two secondary windings with different connection schemes. The simulation results confirmed that the proposed substation topology provides the voltage and current harmonics level on the substation power busbars in accordance with the IEEE Standard 519-2014 requirements over the entire frequency range of the fans' motor control.

Keywords: gas cooling plant; power supply system; frequency variable drive; power quality; harmonic compensation



Citation: Yerbayev, Y.; Artyukhov, I.; Zemtsov, A.; Artyukhov, D.; Molot, S.; Japarova, D.; Zakharov, V. Negative Impact Mitigation on the Power Supply System of a Fans Group with Frequency-Variable Drive. *Energies* **2022**, *15*, 8858. <https://doi.org/10.3390/en15238858>

Academic Editor: Juri Belikov

Received: 23 October 2022

Accepted: 21 November 2022

Published: 23 November 2022

Publisher's Note: MDPI stays neutral with regard to jurisdictional claims in published maps and institutional affiliations.



Copyright: © 2022 by the authors. Licensee MDPI, Basel, Switzerland. This article is an open access article distributed under the terms and conditions of the Creative Commons Attribution (CC BY) license (<https://creativecommons.org/licenses/by/4.0/>).

1. Introduction

There is a wide range of technological installations including groups of fans. For example, cooling towers cool recycled water at thermal power plants, oil refineries, and petrochemical and other industrial enterprises [1]. A large number of fans contain gas cooling plants (GCPs), providing the required temperature regime of the main gas transport. The main structural element of the GCP is the air-cooling unit (ACU). Electrically driven fans pump air through their heat-exchange sections [2]. GACs, where fans are placed under heat-exchange sections and are driven by multipole asynchronous motors, have become widespread. Figure 1 shows the GCP, which consists of 6 GACs, type 2AVG-75. These GACs have two VASO-16-14-24 electric motors in their composition with fans on the shaft. The rated power of the motor is 37 kW; rotation speed of the fans wheels is about 250 rpm.

A GCP can include 24 or more electrically driven fans. The total power consumed by a single gas cooling plant alone amounts to hundreds of kilowatts. Therefore, a considerable

amount of electricity is used to cool the gas. Power consumption for gas cooling after compression can reach 50–70% of total power consumption for gas transportation depending on climatic conditions [3]. Thus, gas cooling cost reduction is an actual problem, which can be solved in the following interrelated directions:

- Improving the aerodynamic characteristics of fans;
- Improving the design of heat exchange sections;
- Improving the algorithms and technical means of fan motor control.

GCP is a complex multidimensional system that implements the energy transfer functions in a distributed heat exchanger. The dependence of the gas temperature at the GCP outlet in the general case is:

$$T_{out} = \Psi(T_{in}, G_{gas}, \Theta_{air}, G_{air}, R_{\Theta}), \quad (1)$$

where

T_{in}, G_{gas} —temperature and mass flow rate of gas at the GCP inlet, respectively;
 Θ_{air}, G_{air} —temperature and mass flow rate of air through the GCP heat exchange sections;
 R_{Θ} —thermal resistance, characterizing the pollution level of the heat exchange surface.

The gas flow rate and temperature after compression, as well as the pollution level of the heat exchanger surfaces, are slow-moving disturbing influences. Outdoor temperature variations (daily and seasonal) are rapidly changing disturbing factors. It follows from (1) that the required gas temperature T_{out} at the GCP outlet can be provided by changing the cooling air mass flow rate G_{air} , which is determined by the sum of the cooling air mass flow rates created by simultaneously operating M fans:

$$G_{air} = \sum_{k=1}^M G_{air.k}. \quad (2)$$

In this case, the fan performance depends on the rotational speed n_k of the fan impeller, the blade angles α_k , and the air temperature Θ_{air} .

The simplest GCP control algorithm involves controlling the mass flow rate (2) by changing the number M of fans running simultaneously. A typical power supply scheme for such a control algorithm is shown in Figure 2. Two 6(10)/0.4 kV transformers are installed at the substation to ensure the required reliability of power supply. The voltages from the secondary windings of the transformers are fed through circuit breakers QF1, QF2 to the corresponding busbar sections, which can be connected through a sectional switch QF3.



Figure 1. Gas cooling plant (a) and VASO-16-14-24 electric motor with a fan on shaft (b).

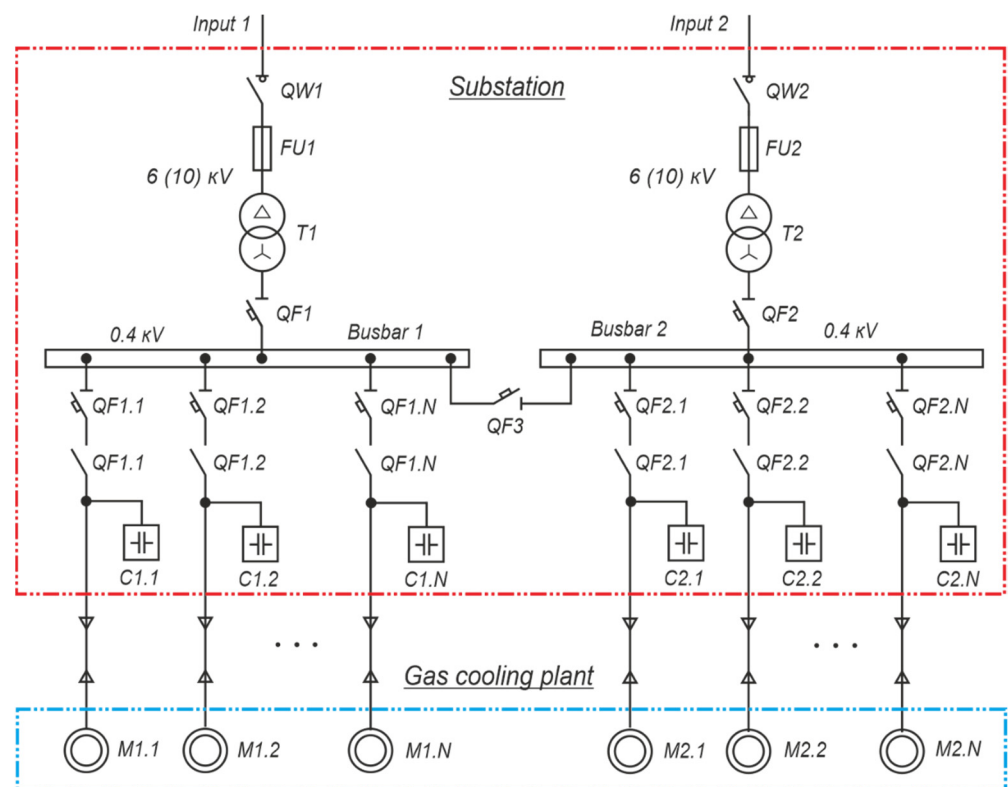


Figure 2. Typical power supply scheme for gas cooling plant.

Electric motors $M1.1...M1.N$ and $M2.1...M2.N$ are powered via cables laid on trestle bridges and are connected to 0.4 kV section buses via circuit breakers $QF1.1...QF1.N$, $QF2.1...QF2.N$ and contactors $K1.1...K1.N$, $K2.1...K2.N$. Capacitors $C1.1...C1.N$ and $C2.1...C2.N$ are connected in parallel to the stator windings to compensate the reactive power of electric motors. Centralized reactive power compensation on busbar sections is also possible.

The discrete motor control algorithm has significant disadvantages. Due to the design features of the GAC, when the fan is running, part of the air blows back through the adjacent fan that is not running if the flow is sufficiently strong to ensure rotating in the opposite direction. Air recirculation has a major impact on the energy efficiency of the gas cooling process, increasing electrical energy losses and reducing overall plant efficiency. In addition, the subsequent direct start of the fan motor rotating in antiphase causes electrical and mechanical shock loads, much higher than the nominal allowed for the motor-fan system. Serious loads on the fan components create a short-term power outage, as a result of which the fan shuts down and restarts after the power supply is restored.

A special feature of the GCP (Figure 1) is the use of multiple asynchronous motors with a power factor of 0.65 to 0.68 in nominal mode. The starting current ratio of such motors is 4.5 to 5. The high inertia of the rotating masses leads to a slow start. A large amount of electrical energy is used to change the mechatronic system kinetic energy. The simultaneous activation of several fans, e.g., after a power outage, is impossible because the power source is overloaded and the protection is triggered.

Methods and technical solutions to reduce starting currents are well known for induction motors with a small number of pole pairs [4,5]. However, they do not have a positive effect for multipole induction motors. Experiments with the soft starter showed that the engine would first start accelerating and then “hang” at an intermediate speed. In spite of the long time, the engine did not go to the set mode. It has been suggested this happens due to the low value of the multipole motor power factor at the starting mode.

Figure 3 shows graphs of changes in apparent power S and its active P and reactive Q components during start-up of an induction motor with a fan on the shaft [6]. Rated motor power is 37 kW, number of pole pairs is 12. Diameter of fan wheel is 5 m.

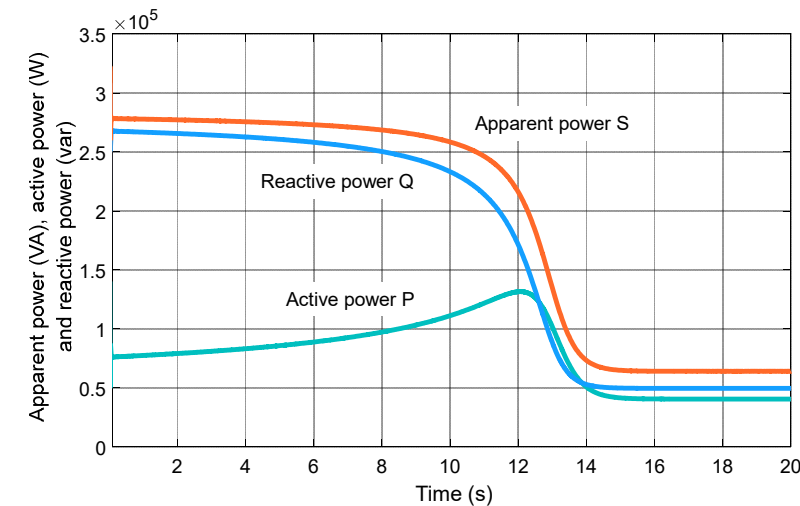


Figure 3. Changes of the active, reactive, and apparent power in the starting motor process.

Reactive power is several times higher than active power at the stages of induction motor magnetic field formation and rotor speed increases. Therefore, the solution to the problem is to use a device that performs controlled compensation of motor reactive power at the starting mode [7].

GCPs, where temperature mode is changed by fans' frequency control, provide more efficient use of electric power [8–10]. Hereinafter, we will use the term frequency-controlled gas cooling plant (FCGCP).

In general, fan impellers can rotate at different frequencies. However, experimental results have shown the turbulence of the cooling “wind field” must be removed in order to increase the efficiency of heat transfer processes in GCP sections. This requires all GCP fans to rotate at the same frequency, which is generated by the control system. The principle of gas temperature control is explained in the graphs in Figure 4 [11].

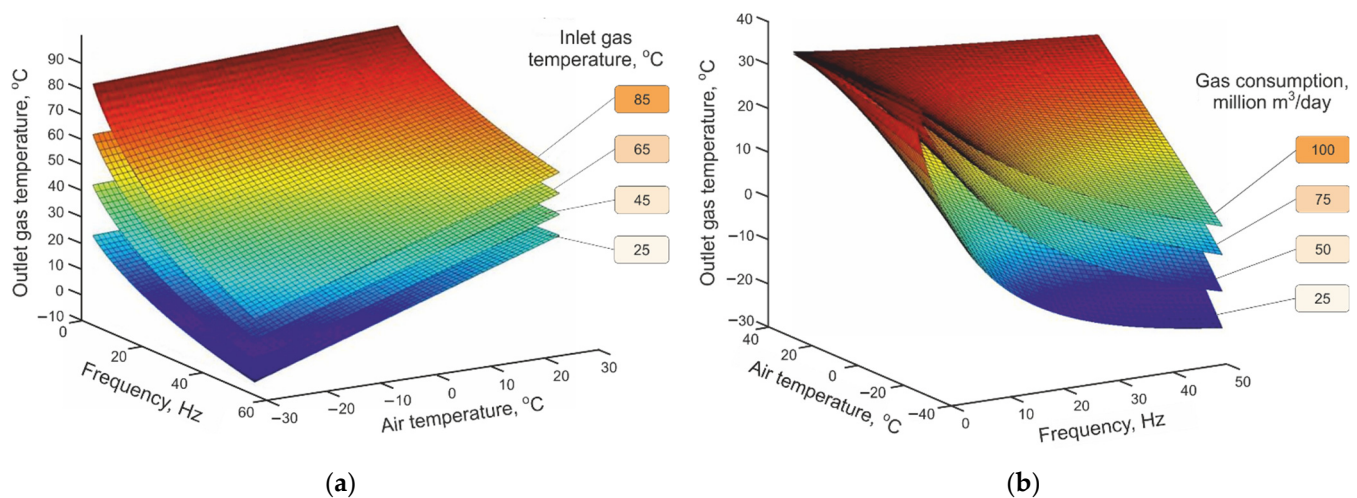


Figure 4. Dependencies of GCP outlet gas temperature on motor control frequency and ambient temperature: (a) at different GCP inlet gas temperatures; (b) at different mass flow rates of the cooled gas.

Let us assume the gas temperature T_{out} at the GCP outlet corresponded to the set value. Then, if the process parameters (T_{in}, G_{gas}) remain unchanged, the ambient air temperature Θ_{air} increases. This leads to an increase in the gas temperature T_{out} at the GCP outlet. The graphs in Figure 4 show that in order to restore the required gas temperature value, it is necessary to increase the frequency f of the voltage applied to the stator windings of electric motors. Thus, to stabilize the temperature T_{out} at the GCP output, the increments of the disturbing influences $\Delta T_{in}, \Delta G_{gas}, \Delta \Theta_{air}$ and the regulating influence Δf must have opposite signs.

The power supply scheme of GCP with a frequency-controlled electric drive of fans is shown in Figure 5. Frequency converters (FCs) FC1.1...FC1.N, FC2.1...FC2.N are connected to 0.4 kV busbar sections through switching devices QF1.1...QF1.N, QF2.1...QF2.N and line chokes L1.1...L1.N, L2.1...L2.N to control GCP fan motors.

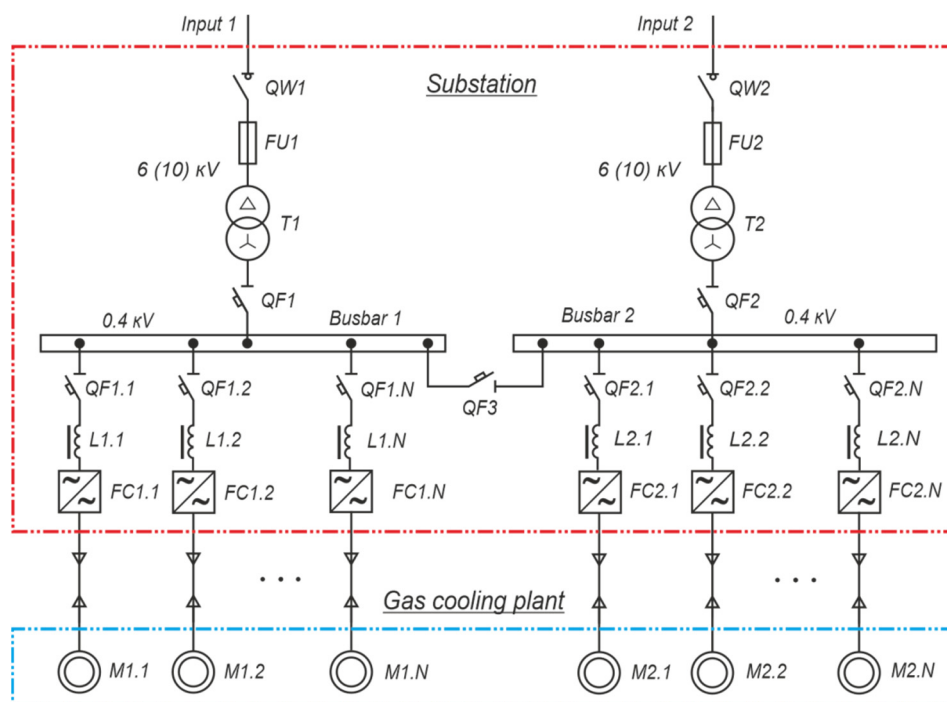


Figure 5. Power supply scheme for gas cooling plant with frequency variable drive of fans.

Connecting a large number of FCs to the substation busbars causes a powerful consumption of non-sinusoidal current. This is explained by the fact that modern frequency converters for motor control are made according to the scheme: rectifier—smoothing filter—autonomous voltage inverter on IGBT-modules. Capacitors are used as a smoothing filter, so the FC input current has a pulsed character with the dominance of the 5th and 7th harmonics [12,13].

Thus, there is a problem of electromagnetic compatibility (EMC) of the FCGCP substation for power supply with power sources and other electrical consumers of the compressor station. The problem of EMC gets worse if the compressor station power supply is coming from an autonomous power source, particularly from a gas turbine power plant [14].

The power source overloads occur when the motors start, causing voltage dips while using the discrete fan control method. With frequency variable fans, the GCP drive consumes a non-sinusoidal current whose magnitude and harmonic composition depend on the operating mode of the plant. The power quality indicators, characterizing the voltage form, go beyond the limits (set by the regulations, for example, Standard 519-2014 [15]) at a certain parameter ratio of power sources and GCP electric drives.

Given the relevance of the problem, the aim of this research is to develop a technical solution, the use of which can reduce the negative impact of the substation with a load in

the form of a group of frequency-variable drives on the power source. To reach this aim, it is necessary to investigate the situation in detail with the application of typical solutions. The investigation tool is an adequate model, which for different operating modes of electric drives allows us to obtain data on the spectral composition of voltages and currents at the substation power buses. Next, based on the results obtained and the world experience in the field of EMC in power supply systems with a frequency-variable drive, it is necessary to propose a technical solution that allows us to reduce the harmonics of voltages and currents to values that are defined by regulatory documents. In this case, the required result should be achieved with minimal financial costs at the stages of implementation and operation, while maintaining other indicators, including reliability.

The problem of harmonic compensation in power supply systems with non-linear electric consumers, including variable-frequency drives, has been studied in a large number of papers. One way of solving the EMC problem involves the use of passive filters. Solution options are described in detail in [16–18]. For the studied object, the passive filters can be connected to the 0.4 kV buses of the substation. However, there is a risk of resonance phenomena.

Active harmonic filters (AHFs) allow for solving EMC problems more effectively [19–22]. When reconstructing a GCP that is in operation, this option may be appropriate, since the installation of the AHF does not require complex construction and installation work. The disadvantage of this solution is the high cost of AHF.

When FCGCP is designed for a new facility, it makes sense to use FCs that use active rectifiers on fully controlled power switches [23,24]. However, this solution also significantly increases the cost of the substation's electrical equipment.

Multipulse rectifiers are a good solution for creating converters with a reduced distorting effect on the power supply system [25–29]. The operating principle of such rectifiers assumes the presence of multi-winding transformers. For this reason, multipulse rectifier circuits are appropriate when it is necessary to change the value of the supply voltage. The FCGCP power supply system requires a reduction of the 6(10) kV line voltage to the value necessary to operate the electric drives. Therefore, the multipulse rectification option can achieve a positive effect.

This paper is structured as follows. Section 2 outlines the approach to modeling the power supply system for a group of frequency variable drives and presents the results of a study on the influence of a typical FCGP on the power source. In Section 3, a new substation topology for FCGP power supply is proposed and the simulation results confirming the positive effect of this solution are provided. Section 4 discusses the results obtained and provides future directions for the work. Finally, the conclusion is provided in Section 5.

2. Impact of the Typical FCGCP on the Power Supply System

2.1. Basic Theoretical Provisions

The mechanism of line voltage distortion can be explained by the scheme in Figure 6. One phase of the power source is represented as an equivalent bipolar with EMF $e(t)$, inductance L_0 and resistance R_0 . A load as a GCP power supply substation is connected to the power source, which consumes current $i(t)$ from the grid.

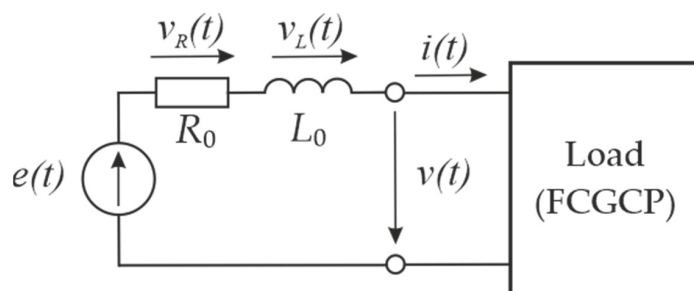


Figure 6. Calculation diagram for one phase of the FCGCP power supply system.

The following equation can be written for the instantaneous voltage value $v(t)$:

$$v(t) = e(t) - v_R(t) - v_L(t), \quad (3)$$

where $v_R(t) = R_0 \cdot i(t)$, $v_L(t) = L_0 \cdot \frac{di(t)}{dt}$ —voltage drop on the resistance and inductance.

If the EMF of the power source $e(t)$ and the load current $i(t)$ are sinusoidal, as in the case of discrete GCP fan control, then the voltage $v(t)$ is also sinusoidal. The effective value of this voltage differs from the effective value of EMF by the voltage drop across the elements R_0 and L_0 connected in series.

When the GCP is equipped with a frequency-controlled fan drive, a non-sinusoidal current $i(t)$ is consumed from the power source. Current flowing through the elements R_0 and L_0 creates non-sinusoidal voltage drops on them. Therefore, even in the case of a sinusoidal EMF according to expression (3), the voltage $v(t)$ will be non-sinusoidal. The distortion of the voltage curve $v(t)$ depends on the relationship between the power supply and the load [30].

Equation (3) in complex form for the n -th harmonic of the line voltage is:

$$\underline{V}_n = \underline{E}_n - (R_0 + jn\omega_1 L_0) \cdot \underline{I}_n = \underline{E}_n - \underline{Z}_n \cdot \underline{I}_n; \quad n = 1, 2, 3, \dots \quad (4)$$

where \underline{E}_n , \underline{V}_n , \underline{I}_n —the harmonic complexes of EMF, voltage, and current with the numbers n ; \underline{Z}_n —the resistance complex of the power source at the n -th harmonic.

If the EMF $e(t)$ is sinusoidal, then Equation (4) for all harmonics with numbers $n \geq 2$ takes the form:

$$\underline{V}_n = -(R_0 + jn\omega_1 L_0) \cdot \underline{I}_n = -\underline{Z}_n \cdot \underline{I}_n. \quad (5)$$

Thus, the effective value of the n -th harmonic of the power source voltage for this situation is determined by the equation:

$$V_n = Z_n \cdot I_n. \quad (6)$$

The GCP with variable-frequency-drive fans is a dynamically changing system; its power source effect depends on many factors. Therefore, it is necessary to determine the conditions under which the influence of the FCGCP on the power supply system becomes critical, and make a decision how to solve the problem. This requires information about the harmonic composition of the current consumed by the GCP from the power source in various operation modes.

It is advisable to choose a solution to the problem of EMC in the power supply system of FCGCP based on the IEEE Standard 519-2014 [15]. This document does not regulate only non-sinusoidal voltage values. Compared to other standards, it regulates the current distortion limits of powerful consumers.

According to IEEE 519-2014, total harmonic distortion (THD) of voltage on power systems rated 1 kV through 69 kV is limited to 5%, with each individual harmonic limited to 3%.

Voltage THD is calculated by the formula:

$$\text{THD} = \frac{\sqrt{U_2^2 + U_3^2 + U_4^2 + U_5^2 + \dots}}{U_1} \cdot 100\%. \quad (7)$$

Current distortion limits are ranked in relation to I_{SC}/I_L ratio on point of common coupling (PCC), where I_{SC} —maximum short-circuit current at PCC, I_L —maximum demand load current (fundamental frequency component) at the PCC under normal load operating conditions. Current distortion limits for power supply systems rated 120 V through 69 kV are provided in Table 1. All values should be in percent of the maximum demand current, I_L . Therefore, even harmonics are limited to 25% of the odd harmonic limits above.

Table 1. Maximum harmonic current in percent of I_L .

I_{SC}/I_L	Individual Harmonic Order (Odd Harmonics)					TDD
	$3 \leq n < 11$	$11 \leq n < 17$	$17 \leq n < 23$	$23 \leq n < 35$	$35 \leq n < 50$	
<20	4.0	2.0	1.5	0.6	0.3	5.0
20 < 50	7.0	3.5	2.5	1.0	0.5	8.0
50 < 100	10.0	4.5	4.0	1.5	0.7	12.0
100 < 1000	12.0	5.5	5.0	2.0	1.0	15.0
>1000	15.0	7.0	6.0	2.5	1.4	20.0

The IEEE 519-2014 standard for current also regulates the total demand distortion (TDD), which is calculated by the formula:

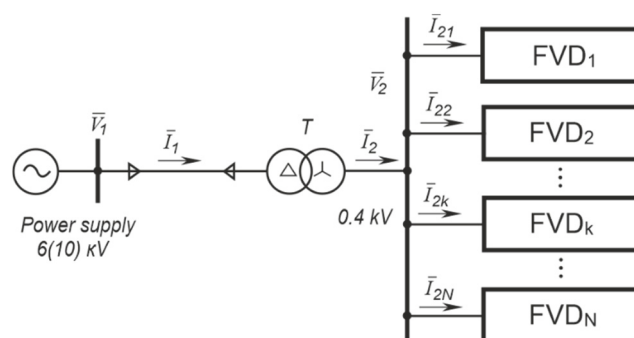
$$\text{TDD} = \frac{\sqrt{I_2^2 + I_3^2 + I_4^2 + I_5^2 + \dots}}{I_L} \cdot 100\%. \quad (8)$$

The row in Table 1, which shows the values of individual harmonics when $I_{SC}/I_L < 20$, is of major interest for the studied object. The situation $I_{SC}/I_L = 20$ corresponds to the practically important case, when one of the inputs of the substation for FCGCP power supply is connected to a transformer 110/6(10) power of 10 MVA. In these cases, EMC problems in the power supply system become visible. When the FCGCP is powered by off-line sources, the I_{SC}/I_L ratio becomes even smaller.

2.2. Modeling the FCGCP Power Supply System

We need a model that reflects the electric drive features as a power-source load to study power-quality issues in the power supply system of a compressor station when GCP is equipped with a frequency-controlled electric drive of fans.

The calculation diagram for one section of the substation busbars, supplying power to the FCGCP, is shown in Figure 7.

**Figure 7.** Calculation scheme for one busbar section.

For example, N electric drives are connected to the 0.4 kV busbar section, and each of them consumes a vector of non-sinusoidal currents \bar{I}_{2k} . The secondary current of transformer T will be equal to the sum of these currents:

$$\bar{I}_2 = \sum_{k=1}^N \bar{I}_{2k}. \quad (9)$$

The voltage on the secondary side of the transformer is characterized by the vector \bar{V}_2 . Its components, according to (3)–(5), have a non-sinusoidal shape. A vector of non-sinusoidal currents \bar{I}_1 is drawn from the power supply; as a result, the components of the vector \bar{V}_1 also have a non-sinusoidal shape.

Each of the N drives can be represented by an equivalent scheme, which is shown in Figure 8. In this scheme: L_{sk} , R_{sk} —inductance and resistance of the line choke, respectively, which can be installed at the input of the k -th FC to ensure EMC standards; C_k , L_{dk} , R_{dk} —capacitance, inductance and resistance of the smoothing choke at the rectifier output, respectively; $R_{inv.k}$ is the equivalent input resistance of the inverter on the k -th FC.

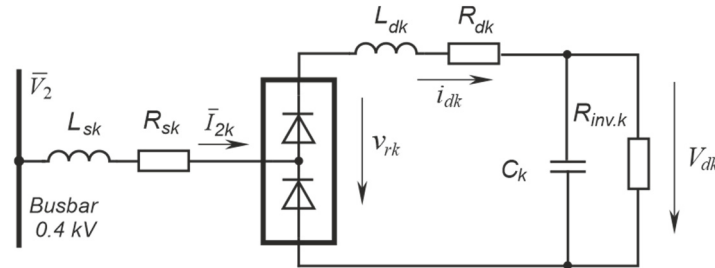


Figure 8. Calculation scheme of the variable-frequency drive.

The inverter presentation as the equivalent input resistance $R_{inv.k}$ is valid because the purpose of the electrical complex modeling is to analyze the influence of canonical harmonics in the spectrum of current consumed by the FC on the electricity quality on the substation buses. The spectrum of harmonics caused by the IGBT module switching is shifted to the high-frequency region. The analysis of this spectrum requires a model that takes into account the parasitic inductances and capacitances of the elements.

The inverter consumes power, which can be found using the equation:

$$P_k = \eta^{-1} P_{0.k} \cdot (f / f_0)^3 \tag{10}$$

where $P_{0.k}$, η are the rated power and efficiency of the electric motor connected to the inverter, respectively; f_0 , f —nominal and current value of the motor control frequency.

The power that is dissipated on the equivalent resistance:

$$P_k = \frac{V_{dk}^2}{R_{inv.k}} \tag{11}$$

From (8) and (9) we obtain the value of the equivalent resistance of the k -th inverter:

$$R_{inv.k} = \frac{\eta \cdot V_{dk}^2}{P_{0.k} \cdot (f / f_0)^3} \tag{12}$$

Figure 9 shows a simulation model scheme to study electromagnetic processes in one section of a typical GCP power supply system, consisting of 12 gas air-coolers with a frequency-controlled fan drive of 37 kW each. The power of the 10/0.4 kV transformer was 1000 kVA, short-circuit voltage—5.5%.

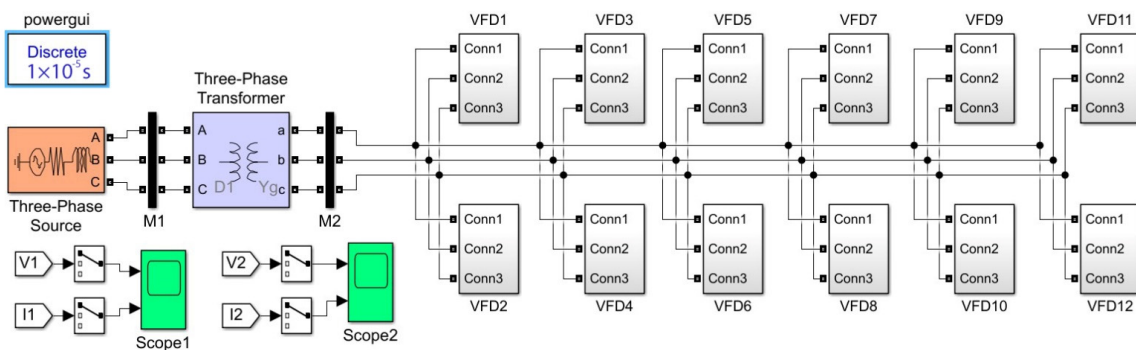


Figure 9. Schematic of the simulation model of a typical power supply system.

A Three-Phase Source unit represents the substation power supply. The Three-Phase Transformer unit simulates a transformer 10/0.4 kV. Simulation models' parameters are shown in Tables A1 and A2.

The schematic of the VFD subsystem is shown in Figure 10. The subsystem consists of a rectifier (Diode Bridge block), line reactors at the rectifier input (Line Reactors block), and a smoothing filter (LD, C blocks). Resistor R, the value of which is calculated by Formula (12), represents the inverter. The motor efficiency was assumed to be 0.915.

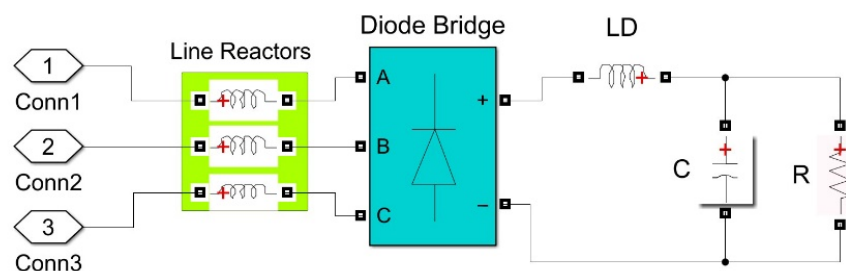


Figure 10. VFD subsystem scheme.

The line chokes inductances were 24 μH . The inductance and capacitance of the smoothing filter were 120 μH and 1000 μF , respectively.

Virtual oscilloscopes Scope 1 and Scope 2 display voltage and current curves. Blocks M1 and M2 (Three-Phase VI Measurements) generate the corresponding signals.

Simulations were performed for a three-phase power source with a voltage of 10 kV and a frequency of 50 Hz, the parameters of which were varied to obtain results for a range of values $I_{SC}/I_L \leq 20$. The control frequency of the fan motors varied from 15 to 50 Hz. The lower limit of the control frequency was adopted based on the conditions to avoid vibration and motors overheating. For each set of parameters f , I_{SC}/I_L virtual oscillograms of phase voltage in PCC and input current in the substation were obtained. Using the built-in MATLAB tool FFT Analysis, the harmonic composition of these curves was investigated.

Figures 11–14 show simulation results for $I_{SC}/I_L = 3.2; 5; 8$ and 20.

The graphs in Figure 11 characterize the non-sinusoidal voltage values in the PCC. They show that harmonics with numbers 5 and 7 appear and increase in the voltage curve spectrum as the fan motor control frequency increases. When $I_{SC}/I_L = 8; 20$ THD is in the acceptable range. If $I_{SC}/I_L = 3.2; 5$, then at certain frequencies of motor control THD exceeds the value of 5%. Voltage harmonics with numbers 7 and above at all I_{SC}/I_L values are less than 3%. The 5th harmonic reaches this value at $f = 47$ Hz for $I_{SC}/I_L = 5$ and at $f = 42$ Hz for $I_{SC}/I_L = 3.2$.

The graphs in Figure 12 show that the greatest contribution to the distortion of the current curve shape is made by the 5th and 7th harmonics. The relative values of these harmonics actually exceed the permissible value of 4% in the entire range of motor control frequency variation at all I_{SC}/I_L ratios.

The maximum voltage waveform distortion in PCC is observed at motor control frequency $f = 50$ Hz and $I_{SC}/I_L = 3.2$. The substation voltage and input current curves for this set of parameters are shown in Figure 13. The voltage spectrum is shown in Figure 14.

Analysis of the simulation results shows that a radical way to reduce the negative impact of the FCGCP on the power supply system is to minimize the 5th and 7th harmonics in the consumed current. The following section offers a solution to this problem.

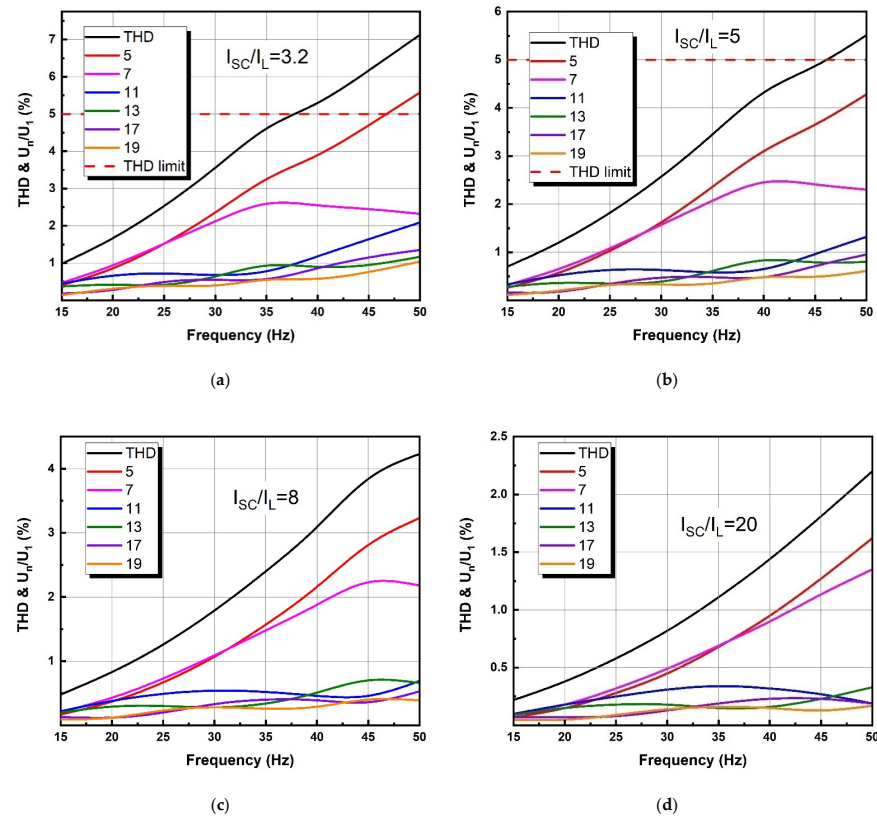


Figure 11. Dependence of voltage THD and voltage harmonics in PCC on motor control frequency in the scheme in Figure 5.

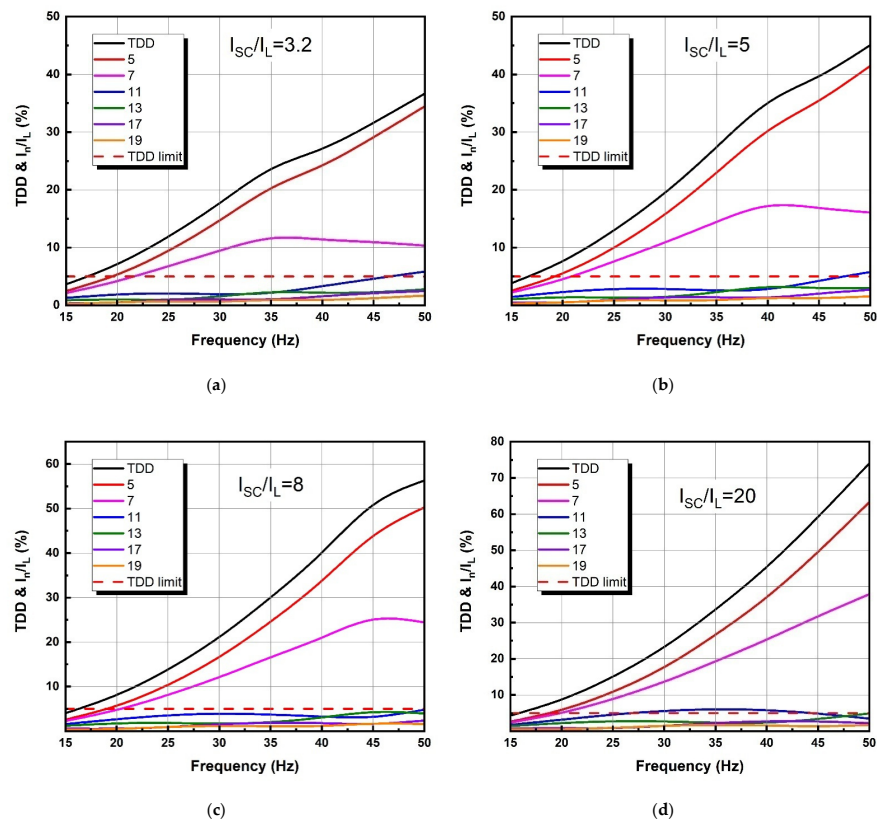


Figure 12. Dependence of current TDD and current harmonics on motor control frequency in the scheme in Figure 5.

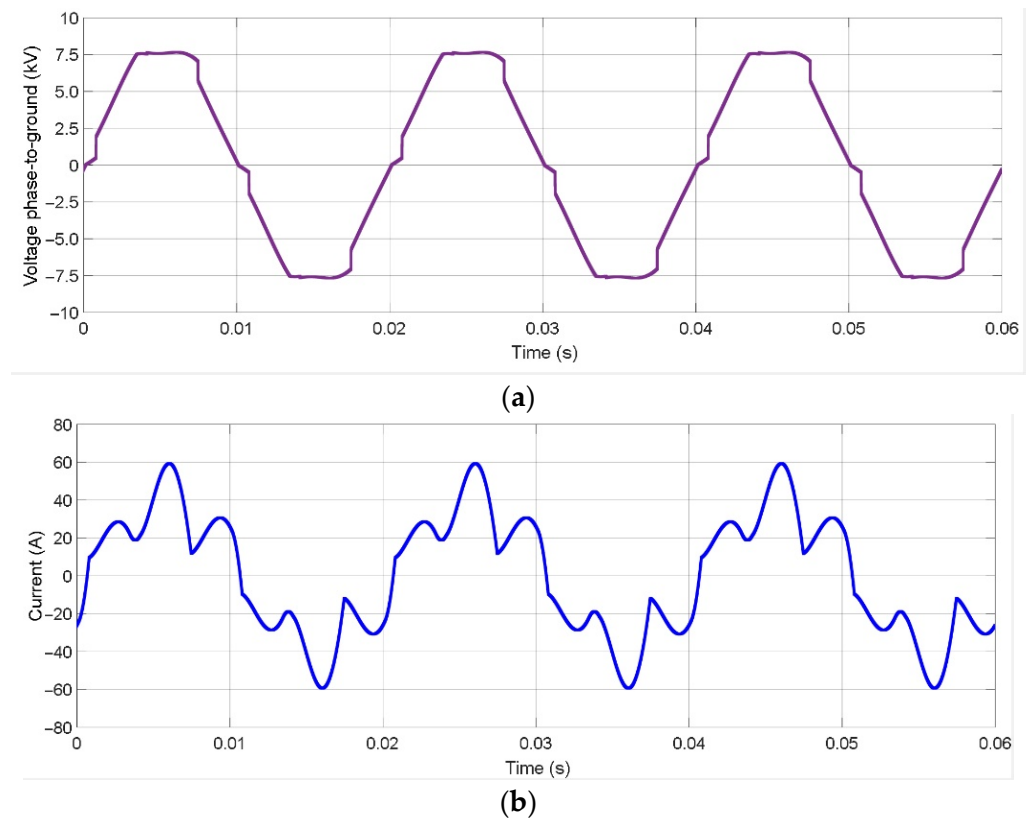


Figure 13. Voltage (a) and current (b) curves in the scheme in Figure 5 at motor control frequency 50 Hz and $I_{SC}/I_L = 3.2$.

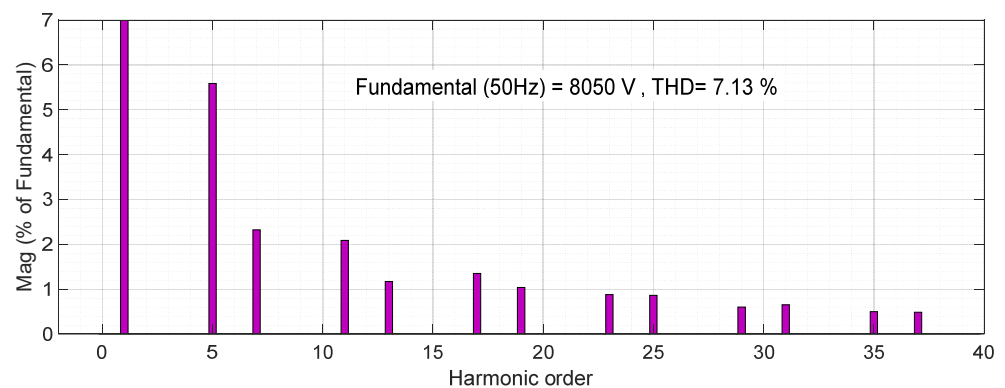


Figure 14. The voltage spectrum in the scheme in Figure 5 at motor control frequency 50 Hz and $I_{SC}/I_L = 3.2$.

3. Novel Substation Topology for Power Supply to the FCGCP

3.1. Proposed Technical Solution

Different options can be considered depending on whether the GCP is an existing facility undergoing renovation or is in the design phase. In any case, the comparison of variants should be made on the condition that the substations have the same spectrum of currents consumed for all FCGCP operation modes.

An effective solution to the EMC problem can be provided by a fundamental change in the substation architecture for FCGCP power supply by organizing DC buses and changing the frequency converters to inverters. As shown in Figure 15, this section consists of transformer and rectifier units [27], which include three-winding transformers T1, T2, and rectifiers AC/DC1.1, AC/DC1.2 and AC/DC2.1, AC/DC2.2. The transformers have

one secondary winding in a star connection and one in a delta connection. The outputs of rectifiers are connected to DC busbar through chokes Ld1 and Ld2, which not only smooth the output voltage ripples, but also serve to eliminate equalizing currents. These currents arise because the output voltage ripples of rectifiers AC/DC1.1 and AC/DC1.2 of one module (AC/DC2.1 and AC/DC2.2 of the other module) are shifted relative to each other by $\pi/6$.

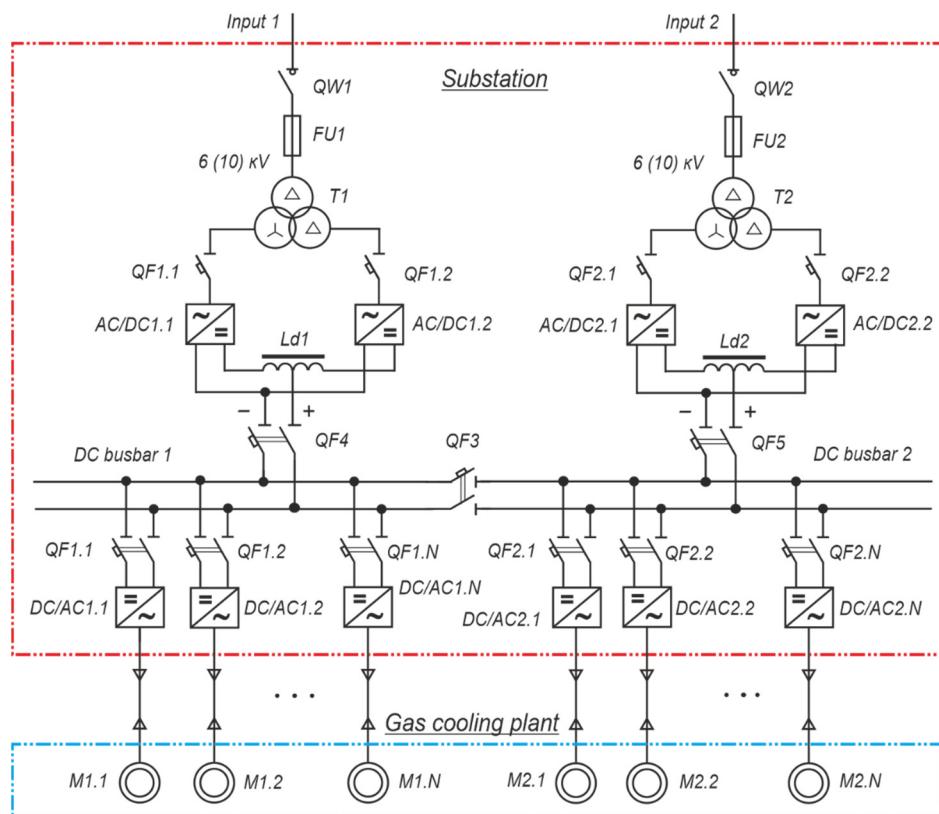


Figure 15. Power supply scheme with three-winding transformers and DC busbars.

DC/AC1.1...DC/AC1.N and DC/AC2.1...DC/AC2.N inverters receive power from the DC link and control the electric motors of M1.1...M1.N, M2.1...M2.N fans. It is necessary to note an important feature of the power supply scheme with the united DC link. Here are the DC-operated switching devices. These are QF1.1...QF1.N and QF2.1...QF2.N circuit breakers for connecting AC/DC1.1...AC/DC1.N and AC/DC2.1...AC/DC2.N inverters to the DC bus. The QF4 and QF5 switchgear, which connect the transformer and rectifier units to the DC bus, as well as the QF3 section switch, also operate on direct current.

Since the secondary winding voltages of transformers T1, T2 are shifted in phase with respect to each other by an angle equal to $\pi/6$, when the secondary winding currents are equal, the 5th and 7th harmonics of magnetic flux are compensated. As a result, these harmonics are also compensated in the primary winding currents of the transformers. The spectrum of currents begins with the 11th harmonic.

3.2. Simulation of the Proposed Electrical Complex

A simulation model in MATLAB with Simulink extension package was developed to study the electrical complex. A simulation model scheme for one busbar section is shown in Figure 16.

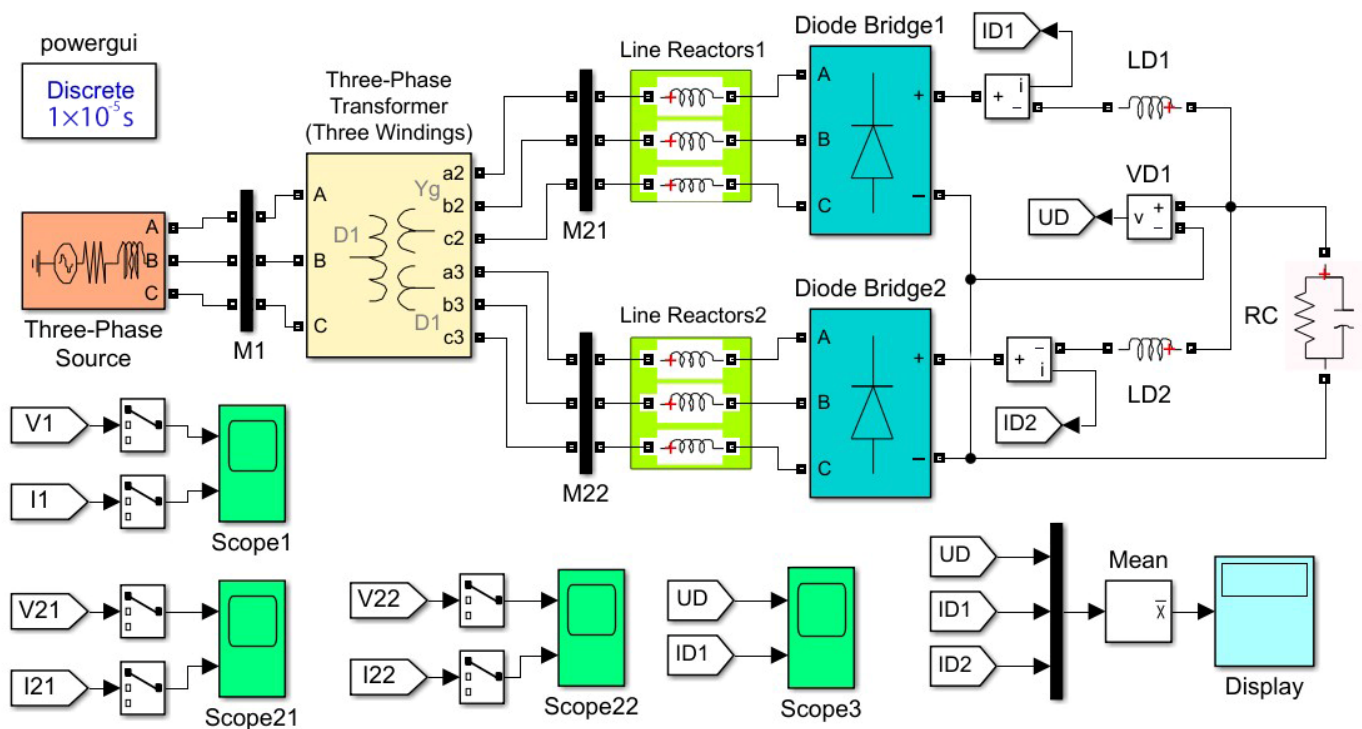


Figure 16. Simulation model scheme of a single busbar section of an electrical complex with an integrated DC link.

A Three-Phase Source unit represents the substation power supply. The Three-Phase Transformer (Three Windings) block is used to simulate a transformer with two secondary windings. Simulation models’ parameters are shown in Tables A1 and A3.

Diode Bridge units model rectifiers. Line Reactors represent the line chokes at the input of the rectifiers. An RC unit as a parallel-connected resistor and capacitor represents the inverters connected to the DC bus. The value of the equivalent resistance R depends on the number of simultaneously working inverters and their load. The formula for its calculation can be obtained using the power balance.

Each of the inverters on the DC bus consumes power, which can be found by Formula (10). Therefore, the total power consumed by a group of N inverters will be determined by the formula:

$$P_{d.in} = \sum_{k=1}^N P_k = \sum_{k=1}^N \eta^{-1} P_{0,k} (f/f_0)^3. \quad (13)$$

If all N drives have the same power, then taking into account (8) and (9) we acquire an expression for calculating the equivalent load resistance R on the DC bus, which is necessary to know in the simulation:

$$R = \frac{\eta \cdot V_{dk}^2}{N \cdot P_{0,k} \cdot (f/f_0)^3}. \quad (14)$$

The Formula (14) shows that the equivalent load resistance on the DC bus decreases when the number of simultaneously connected inverters increases, and increases when the control frequency of the electric motors decreases.

The capacitor capacity, written in the setup window of the RC block of the simulation model in Figure 16, depends on the number of simultaneously working inverters. Therefore, if any inverter is connected to the DC bus, the corresponding filter capacitor is connected.

To calculate the equivalent resistance according to Formula (14), the following conditions are taken: number of variable-frequency drives $N = 12$, rated power of each drive $P_0 = 37$ kW.

A three-phase bridge rectifier forms the DC bus voltage. Therefore, this formula can be used to calculate it:

$$V_d = \frac{3\sqrt{2}}{\pi} V_2 \tag{15}$$

where V_2 is the effective value of voltage on the secondary windings of the transformer.

A 1000 μF filter capacitor is connected in parallel to each inverter, and therefore the total capacitor capacity in the model circuit is $12 \times 1000 = 12000 \mu\text{F}$. The inductance of smoothing reactors LD1 and LD2 is assumed to be 100 μH .

The results of the simulation are shown in Figures 17–20. The control frequency range of the fan motors and the power source parameters were the same as in the circuit analysis in Figure 5.

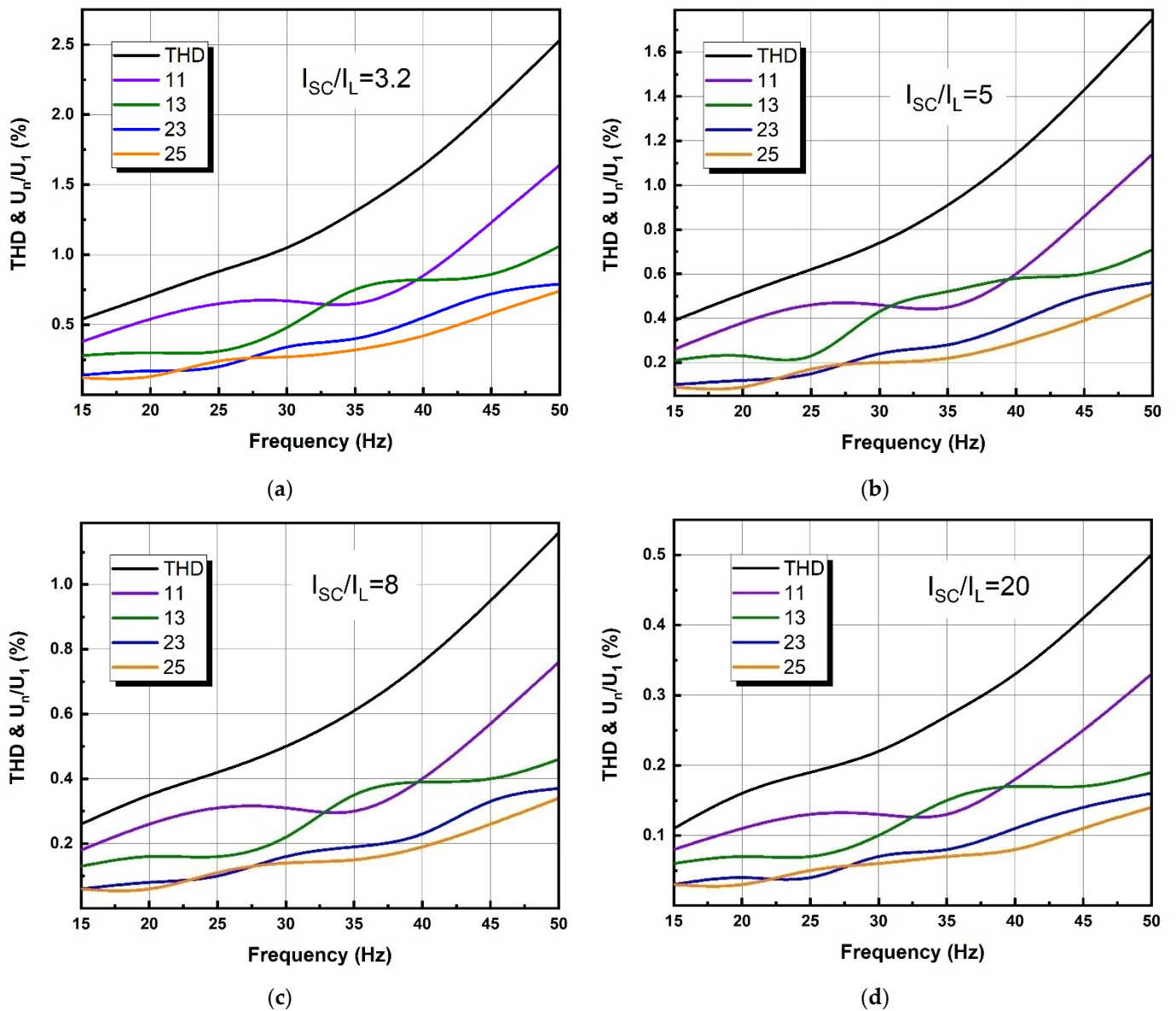


Figure 17. Dependence of THD and voltage harmonics in PCC on motor control frequency in the scheme in Figure 15.

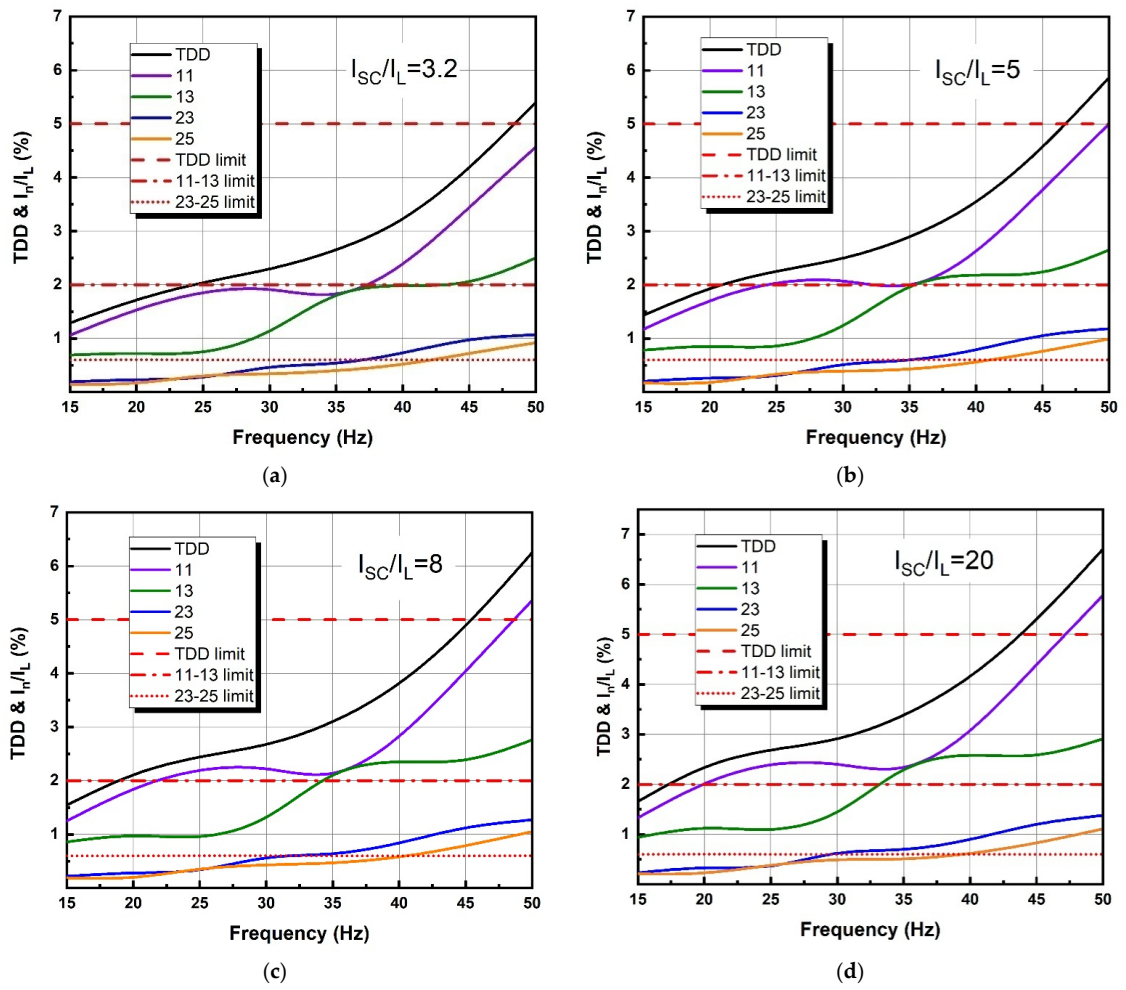


Figure 18. Dependence of TDD and current harmonics on motor control frequency in the scheme in Figure 15.

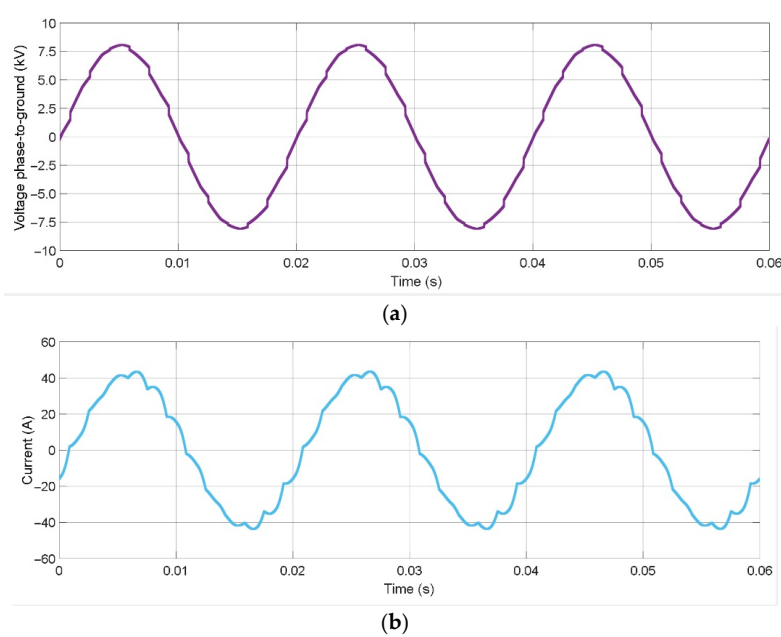


Figure 19. Voltage (a) and current (b) curves in the scheme in Figure 15 at motor control frequency 50 Hz and $I_{sc}/I_L = 3$.

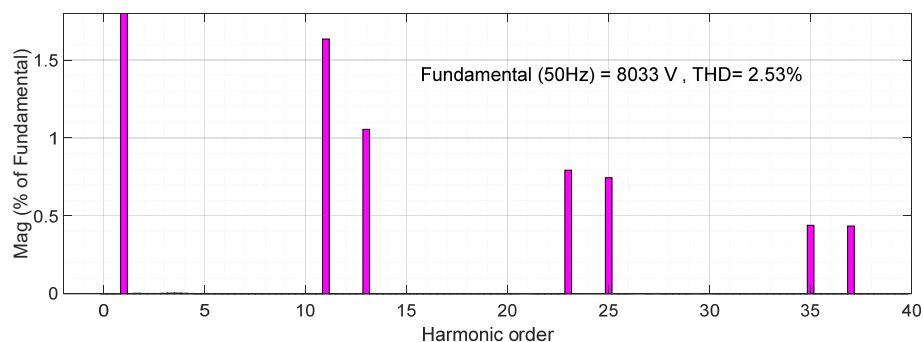


Figure 20. The voltage spectrum in the scheme in Figure 15 at motor control frequency 50 Hz and $I_{SC}/I_L = 3.2$.

The graphs in Figure 17 show that for all values of the I_{SC}/I_L ratio and motor control frequencies, the voltages THD and individual harmonics are in the range established by IEEE Standard 519-2014.

The current TDD (Figure 18) slightly exceeds the allowable value of 5% while controlling motors with frequencies of 45 Hz and above. Exceeding the 11th and 13th harmonics limit of 2% is seen at control frequencies of 35 Hz and above. In this case, the harmonic number 11 requires attention, and therefore, when increasing the control frequency to 50 Hz, this harmonic value ranges from 4.57 to 5.78%. The current harmonics with numbers 23 and 25 have no significant effect on the distortion of the voltage curve in the PCC.

Substation voltage and input current curves at motor control frequency $f = 50$ Hz and $I_{SC}/I_L = 3.2$ ratio are shown in Figure 19. The spectral content of the voltage is shown in Figure 20.

4. Discussion

The results of modeling are the basis for making a decision on the option to ensure EMC in the power supply system of a group of fans with a frequency-controlled drive. As mentioned above, the option is determined by the current situation.

If GCP fans are equipped with a frequency-variable drive on a running plant, installation of active filters or the use of frequency converters with active rectifiers is an effective solution. Both options require large capital expenditures, but they can start working quickly enough.

The option of changing the architecture of the substation to supply power to the FCGCP by organizing DC buses, replacing FC with inverters and using transformers with two secondary windings is much cheaper. The substation cost increase is only due to the increased cost of transformers and the need to purchase and install rectifiers with equalizing reactors. Some increase in the cost of the substation will occur due to the use of DC switching equipment. The disadvantages of this option include a large amount of construction and installation work, and the replacement of transformers' and rectifiers' installation. Therefore, this option has certain advantages when designing new gas transmission facilities.

Further direction of research involves modeling and study of transients during start-up of electric motors and changes in their operation mode.

5. Conclusions

The negative impact reduction on the power supply system of a group of fans with a variable-frequency drive is an urgent task. Its solution makes it possible to ensure the required quality of electricity. The article studies the effect of a frequency-controlled gas cooling plant on a power-limited source and proposes a solution to reduce it. The authors propose changing the architecture of the substation for FCGCP power supply by organizing DC buses, replacing the FC with inverters, and using transformers with two secondary

windings with different connection schemes. The advantage of this option is the following: While supplying the substation from an autonomous power source, at which the output voltage frequency is subjected to changes, the proposed option in any situation provides full compensation of harmonics with numbers 5, 7, 17, and 19 in the current consumption curve. These positive properties of the proposed solution can be applied most effectively in the design and construction of new gas transmission facilities.

Author Contributions: Conceptualization, I.A.; methodology, I.A.; software, D.A. and I.A.; validation, I.A. and D.A.; formal analysis, S.M.; investigation, A.Z.; resources, Y.Y. and V.Z.; data curation, V.Z. and D.J.; writing—original draft preparation, I.A. and D.A.; writing—review and editing, I.A.; visualization, D.A. and I.A.; supervision, Y.Y. and S.M.; project administration, I.A. All authors have read and agreed to the published version of the manuscript.

Funding: This research received no external funding.

Data Availability Statement: Not applicable.

Conflicts of Interest: The authors declare no conflict of interest.

Abbreviations

The following abbreviations are used in this manuscript:

Abbreviations

ACU	Air-cooling unit
AHF	Active harmonic filter
EMC	Electromagnetic compatibility
EMF	Electromotive force
FC	Frequency converter
FCGCP	Frequency-controlled gas cooling plant
FFT	Fast Fourier transformation
GCP	Gas cooling plant
IGBT	Insulated Gate Bipolar Transistors
PCC	Point of common coupling
TDD	Total demand distortion
THD	Total harmonic distortion
VFD	Variable-frequency drive

Nomenclature

P	Active power
Q	Reactive power
S	Apparent power
T_{in}	Temperature of gas at the GCP inlet
G_{gas}	Mass flow rate of gas at the GCP inlet
Θ_{air}	Temperature of air through the GCP heat exchange sections
G_{air}	Mass flow rate of air through the GCP heat exchange sections
R_{Θ}	Thermal resistance
T_{out}	Gas temperature at the GCP outlet
$e(t)$	Electromotive force
$v(t)$	Voltage on the load
$v_R(t)$	Voltage on the resistance
$v_L(t)$	Voltage on the inductance
$i(t)$	Current consumed from the grid
\bar{V}_1	Grid voltages vector
\bar{I}_1	Grid currents vector
\bar{V}_2	Busbar 0.4 kV voltage vector
\bar{I}_2	Secondary currents vector
f_0	Nominal value of the motor control frequency
f	Current value of the motor control frequency
$P_{0.k}$	Rated power of the electric motor
P_k	Electric motor power at control frequency f
η	Efficiency of the electric motor

V_2	RMS voltage on the transformer secondary winding
V_d	DC busbar voltage
$P_{d.in}$	Power consumed by a group of N inverters
$R_{inv.k}$	Value of the equivalent resistance of the k -th inverter
L_{sk}	Inductance of the line choke
R_{sk}	Resistance of the line choke
C_k	Capacitance of the smoothing choke at the rectifier output
L_{dk}	Inductance of the smoothing choke at the rectifier output
R_{dk}	Resistance of the smoothing choke at the rectifier output

Appendix A

Table A1 shows the simulation model parameters for the energy source in Figures 9 and 16. Tables A2 and A3 show the simulation model parameters for the transformers in Figures 9 and 16, respectively.

Table A1. Simulation model parameters for the Three-Phase Source block.

Parameter	Value	Unit
Phase-to-phase rated voltage	10	kV
Frequency	50	Hz
Source resistance	0.2 ... 1.33	Ω
Source inductance	$(3 \dots 18.75) \times 10^{-3}$	H

Table A2. Simulation model parameters for the Three-Phase Transformer block in Figure 9.

Parameter	Value	Unit
Rated power	1000	kVA
Frequency	50	Hz
Winding 1 parameters		
Phase-to-phase rated voltage	10	kV
Winding resistance	1.05	Ω
Leakage inductance	17.5×10^{-3}	H
Winding 2 parameters		
Phase-to-phase rated voltage	0.4	kV
Winding resistance	0.004	Ω
Leakage inductance	28×10^{-6}	H
Magnetization parameters		
Resistance	16×10^3	Ω
Inductance	22.5	H

Table A3. Simulation model parameters for the Three-Phase Transformer block in Figure 16.

Parameter	Value	Unit
Rated power	1000	kVA
Frequency	50	Hz
Winding 1 parameters		
Phase-to-phase rated voltage	10	kV
Winding resistance	1.05	Ω

Table A3. Cont.

Parameter	Value	Unit
Leakage inductance	17.5×10^{-3}	H
Winding 2 parameters		
Phase-to-phase rated voltage	0.4	kV
Winding resistance	0.012	Ω
Leakage inductance	84×10^{-6}	H
Winding 3 parameters		
Phase-to-phase rated voltage	0.4	kV
Winding resistance	0.004	Ω
Leakage inductance	28×10^{-6}	H
Magnetization parameters		
Resistance	16×10^3	Ω
Inductance	22.5	H

References

- Kroger, D.G. Air-Cooled Heat Exchangers and Cooling Towers: Thermal-flower Performance Evaluation and Design. Ph.D. Thesis, University of Stellenbosch, Stellenbosch, South Africa, 2004.
- Mokhatab, S.; Poe William, A.; Speight, J.G. *Handbook of Natural Gas Transmission and Processing—Principles and Practices*, 3rd ed.; Elsevier: Amsterdam, The Netherlands, 2015.
- Artyukhov, I.I.; Arshakyan, I.I.; Trimbach, A.A. Analysis of circuits of frequency control of gas-cooling device's fans. In Proceedings of the International Conference on Actual Problems of Electron Devices Engineering, Saratov, Russia, 24–25 September 2008; pp. 381–389. [\[CrossRef\]](#)
- Larabee, J.; Pellegrino, B.; Flick, B. Induction Motor Starting Methods and Issues. In Proceedings of the Record of Conference Papers Industry Applications Society 52nd Annual Petroleum and Chemical Industry Conference, Athens, Greece, 12–14 September 2005; pp. 217–222.
- Habyarimana, M.; Dorrell, D.G. Methods to reduce the starting current of an induction motor. In Proceedings of the International Conference on Power, Control, Signals and Instrumentation Engineering (ICPCSI), Chennai, India, 21–22 September 2017; pp. 34–38. [\[CrossRef\]](#)
- Artyukhov, I.I.; Stepanov, S.F.; Arshakyan, I.I.; Korotkov, A.V.; Pogodin, N.V. Dynamic compensation of reactive power at power supply system for air cooler of gases. *Promyshlennaya Energ.* **2004**, *6*, 47–51.
- Artyukhov, I.I.; Stepanov, S.F.; Mirgorodskaya, E.E.; Mityashin, N.P.; Zemtsov, A.I. Transient Processes with Starting of a Multi-Pole Asynchronous Motor with a Fan on the Shaft. In Proceedings of the 2021 17th Conference on Electrical Machines, Drives and Power Systems (ELMA 2021), Sofia, Bulgaria, 1–4 July 2021; pp. 1–4. [\[CrossRef\]](#)
- Abakumov, A.M.; Kuznetsov, P.K.; Stepashkin, I.P. Adaptive automatic control system for air-cooled gas apparatus. *J. Phys. Conf. Ser.* **2018**, *1111*, 012031. [\[CrossRef\]](#)
- Yanvarev, I.; Vanyashov, A.; Krupnikov, A. Thermal Management Technologies Development for the Gas Transport on the Gas-main Pipeline. *Procedia Eng.* **2015**, *113*, 237–243. [\[CrossRef\]](#)
- Artyukhov, I.; Abakumov, A.; Zemtsov, A.; Yerbayev, Y.; Zakharov, V. Energy Efficiency Analysis of Control Algorithms for Fan Electric Drives in Gas Air-Cooling Plants. In *Lecture Notes in Civil Engineering, Proceedings of ICEPP 2021, Kazan, Russia, 26 February 2021*; Springer: Cham, Switzerland, 2022; Volume 190, pp. 46–55. [\[CrossRef\]](#)
- Artyukhov, I.I.; Stepanov, S.F.; Pylskaya, E.K.; Zemtsov, A.I. Dynamics of Compressed Gas Temperature Stabilization System with Variable-Frequency Drive of Fans in a Gas Air-Cooling Unit. In Proceedings of the International Conference on Electrotechnical Complexes and Systems (ICOECS), Ufa, Russia, 27–30 October 2020; pp. 1–5. [\[CrossRef\]](#)
- Novák, J.; Šimánek, J.; Černý, O.; Doleček, R. EMC of frequency controlled electric drives. *Radioengineering* **2008**, *17*, 101–105.
- Zare, F.; Soltani, H.; Kumar, D.; Davari, P.; Delpino, H.A.M.; Blaabjerg, F. Harmonic Emissions of Three-Phase Diode Rectifiers in Distribution Networks. *IEEE Access* **2017**, *5*, 2819–2833. [\[CrossRef\]](#)
- Artyukhov, I.; Bochkareva, I.; Molot, S.; Kalganova, S.; Stepanov, S.; Trigorly, S. Power Quality in Industrial Isolated Generation Power Systems with Powerful Nonlinear Consumers. In Proceedings of the 9th International Scientific Symposium EL-EKTROENERGETIKA 2017, Stará Lesná, Slovak Republic, 12–14 September 2017; pp. 44–49.
- Standard 519-2014*; IEEE Recommended Practice and Requirements for Harmonic Control in Electric Power Systems. IEEE: New York, NY, USA, 2014.
- Jaafari, K.A.A.; Poshtan, M.; Beig, A.R. Passive wide spectrum filter for variable speed drives in oil and gas industry. In Proceedings of the 11th International Conference on Electrical Power Quality and Utilisation, Lisbon, Portugal, 17–19 October 2011; pp. 1–6.

17. Park, B.; Lee, J.; Yoo, H.; Jang, G. Harmonic Mitigation Using Passive Harmonic Filters: Case Study in a Steel Mill Power System. *Energies* **2021**, *14*, 2278. [[CrossRef](#)]
18. Lumbreras, D.; Gálvez, E.; Collado, A.; Zaragoza, J. Trends in Power Quality, Harmonic Mitigation and Standards for Light and Heavy Industries: A Review. *Energies* **2020**, *13*, 5792. [[CrossRef](#)]
19. Špelko, A.; Blažič, B.; Papič, I.; Herman, L. Active Filter Reference Calculations Based on Customers' Current Harmonic Emissions. *Energies* **2021**, *14*, 220. [[CrossRef](#)]
20. Vitoi, L.; Brandao, D.; Tedeschi, E. Active Power Filter Pre-Selection Tool to Enhance the Power Quality in Oil and Gas Platforms. *Energies* **2021**, *14*, 1024. [[CrossRef](#)]
21. Raman, R.; Sadhu, P.K.; Kumar, R.; Rangarajan, S.S.; Subramaniam, U.; Collins, E.R.; Senjyu, T. Feasible Evaluation and Implementation of Shunt Active Filter for Harmonic Mitigation in Induction Heating System. *Electronics* **2022**, *11*, 3464. [[CrossRef](#)]
22. Shankar, V.A.; Kumar, N.S. Implementation of Shunt Active Filter for Harmonic Compensation in a 3 Phase 3 Wire Distribution Network. *Energy Procedia* **2017**, *117*, 172–179. [[CrossRef](#)]
23. Hudson, R.; Hong, S.; Hoft, R. Modeling and simulation of a digitally controlled active rectifier for power conditioning. In Proceedings of the Sixth Annual Applied Power Electronics Conference and Exhibition, Dallas, TX, USA, 10–15 March 1991; pp. 423–429. [[CrossRef](#)]
24. Chimonyo, K.B.; Kumar, K.S.; Kumar, B.K.; Ravi, K. Design and Analysis of Electrical Drives Using Active Front End Converter. In Proceedings of the 2018 Second International Conference on Inventive Communication and Computational Technologies (ICICCT), Coimbatore, India, 20–21 April 2018; pp. 115–119. [[CrossRef](#)]
25. Vilberger, M.E.; Kulekina, A.V.; Bakholdin, P.A. The twelfth-pulse rectifier for traction substations of electric transport. *IOP Conf. Ser. Earth Environ. Sci.* **2017**, *87*, 032052. [[CrossRef](#)]
26. Qian, G.; Wang, Q.; He, S.; Dai, W.; Wei, N.; Zhou, N. Harmonic Modeling and Analysis for Parallel 12-Pulse Rectifier under Unbalanced Voltage Condition in Frequency-Domain. *Energies* **2022**, *15*, 3946. [[CrossRef](#)]
27. Corti, F.; Shehata, A.H.; Laudani, A.; Cardelli, E. Design and Comparison of the Performance of 12-Pulse Rectifiers for Aerospace Applications. *Energies* **2021**, *14*, 6312. [[CrossRef](#)]
28. Setlak, L.; Kowalik, R. Examination of Multi-Pulse Rectifiers of PES Systems Used on Airplanes Compliant with the Concept of Electrified Aircraft. *Appl. Sci.* **2019**, *9*, 1520. [[CrossRef](#)]
29. Surya, H. The Effect of 12 Pulse Converter Input Transformer Configuration on Harmonics of Input Current. In *IOP Conference Series: Materials Science and Engineering*; IOP Publishing, Bristol, UK, 2021; Volume 1158. [[CrossRef](#)]
30. Shklyarskiy, Y.; Dobush, I.; Carrizosa, M.J.; Dobush, V.; Skamyin, A. Method for Evaluation of the Utility's and Consumers' Contribution to the Current and Voltage Distortions at the PCC. *Energies* **2021**, *14*, 8416. [[CrossRef](#)]